

Wide-band transmittance of one-dimensional photonic crystals carved in $\text{Si}_3\text{N}_4/\text{SiO}_2$ channel waveguides

D. Gerace,^{a)} M. Galli, D. Bajoni,^{b)} G. Guizzetti, and L. C. Andreani
*Istituto Nazionale per la Fisica della Materia (INFN-CNR) and Dipartimento di Fisica "A. Volta,"
 Università di Pavia, via Bassi 6, I-27100 Pavia, Italy*

F. Riboli, M. Melchiorri, N. Daldosso, and L. Pavesi
Dipartimento di Fisica, Università di Trento, via Sommarive 14, I-38050 Povo (Trento), Italy

G. Pucker
*Istituto Trentino di Cultura, Centro per la Ricerca Scientifica e Tecnologica (ITC-IRST),
 Microsystem Division, Via Sommarive 18, I-38050 Povo (Trento), Italy*

S. Cabrini, L. Businaro, and E. Di Fabrizio^{c)}
*TASC-Istituto Nazionale per la Fisica della Materia (INFN-CNR) at ELETTRA, Lilit Beamline,
 S.S. 14-km 163.5, I-34012 Basovizza-Trieste, Italy*

(Received 6 September 2005; accepted 16 October 2005; published online 17 November 2005)

Experimental and theoretical investigations of photonic crystal (PhC) structures in silicon nitride/silicon dioxide ($\text{Si}_3\text{N}_4/\text{SiO}_2$) vertical waveguiding geometry are reported. One-dimensional patterns, either periodic or with cavity layers, are carved onto the channel waveguides by using focused ion beam lithography. Broadband transmittance spectroscopy in the visible and near-infrared frequency ranges is employed to show photonic band gap behavior up to the fourth order. For structures with a cavity layer, resonant peaks appear in transmittance spectra within the photonic gaps, in agreement with theory. The results show the interest of $\text{Si}_3\text{N}_4/\text{SiO}_2$ -based PhC waveguides for photonics applications from the infrared up to the visible range. © 2005 American Institute of Physics. [DOI: 10.1063/1.2135408]

In the last decades there has been common agreement that silicon-based photonics is a key technology to be developed in view of manipulating, controlling, and detecting light at submicrometer length scales.¹ Promising systems in this respect are photonic crystals, where light confinement and propagation is tailored by a periodic dielectric modulation. Owing to technological difficulties in fabricating three-dimensional periodic structures operating at visible wavelengths, photonic crystal (PhC) slabs, where a high-index core layer is sandwiched between lower index claddings, are considered as a promising alternative for a three-dimensional control of light.² In these systems, one- or two-dimensional (1D or 2D) dielectric periodicity in the plane is added to total internal reflection confinement along the vertical direction, with good promise of achieving all-optical integrated circuits.

In the existing literature, two main types of structures may be distinguished depending on the strength of the out-of-plane dielectric mismatch between core and cladding(s) materials. Transmission spectroscopy on silicon-based systems has been already used to characterize the photonic band gap properties of high index contrast structures.^{3–5} On the other hand, weak index contrast PhC slabs have been mainly investigated in GaAs-based structures by using external laser^{6,7} or internal light source⁸ techniques. So far, little work has been made concerning the use of silicon-based PhC slabs that are transparent at visible wavelengths. Transmission measurements on weak index contrast PhC slabs made of a Si_3N_4 core layer sandwiched between SiO_2 claddings have

been shown in Ref. 9, in which the fundamental photonic band gap was investigated for a 2D lattice of air holes. A theoretical study on Bragg waveguide gratings based on such materials is given in Ref. 10.

1D-PhC slabs are the waveguide-embedded analog of the well known Bragg mirrors. Together with PhC slab resonators, i.e., the analog of Fabry-Pérot cavities, they represent key elements for future PhC-based integrated circuits. It is known that PhC slabs support both truly guided modes, whose dispersion falls below the light line of the cladding material, and quasiguided modes falling above the light line.^{6,11–14} The latter suffer from intrinsic out-of-plane losses owing to the in-plane periodic pattern, even in the absence of absorption losses. In the present letter, 1D-PhC waveguides fabricated in a $\text{SiO}_2/\text{Si}_3\text{N}_4/\text{SiO}_2$ vertical geometry are studied by using wide-band transmittance spectroscopy. The main purpose of the work is to show large-spectrum photonic band gap properties of Bragg mirrors and resonators embedded in $\text{Si}_3\text{N}_4/\text{SiO}_2$ PhC slabs. Results presented here show that Si_3N_4 -based PhC slabs may be usefully employed for applications to photonic devices operating up to the visible range.

Low-loss $\text{Si}_3\text{N}_4/\text{SiO}_2$ channel waveguides are produced within a complementary metal-oxide-semiconductor fabrication pilot line by low-pressure chemical vapor deposition (LPCVD).¹⁵ It is known that employing LPCVD reduces interface roughness and, as a consequence, scattering losses. A 2.0 μm cladding layer of boron-phosphor-silicate glass (BPSG) is deposited on a 4 in. Si wafer. Then, a 200-nm-thick Si_3N_4 guiding layer is deposited by a LPCVD process and two-dimensional rib waveguides with 10- μm -wide rectangular cross section are defined by lithography and etching. Channel waveguides are obtained by covering the Si_3N_4 rib with a 500-nm-thick layer of a medium-temperature LPCVD

^{a)}Electronic mail: gerace@fisicavolta.unipv.it

^{b)}Present address: LPN-CNRS, 91460 Marcoussis, France.

^{c)}Present address: Università della Magna Graecia, Campus Germaneto Lab. BIONEM, I-88100 Catanzaro, Italy.

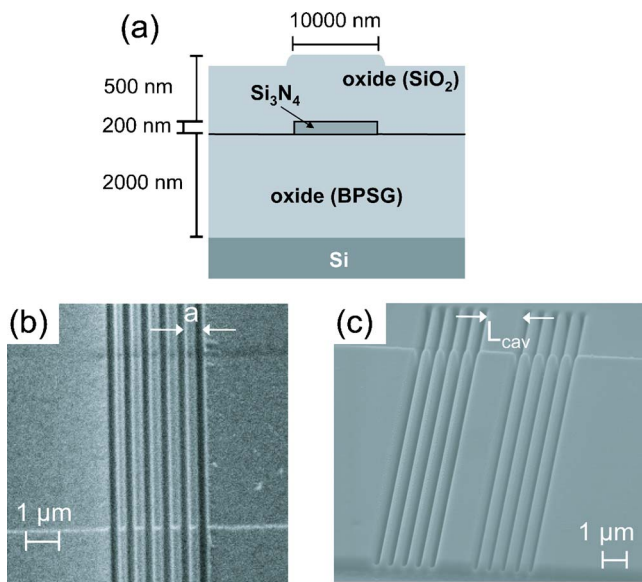


FIG. 1. (Color online) (a) Schematic illustration of the Si_3N_4 channel waveguide. (b) Top view of the waveguide-embedded Bragg mirror with six air slits (FIB image): the lattice constant is $a=525$ nm. (c) SEM image of the sample with a cavity layer between Bragg mirrors with five air slits per side.

tetraethyl orthosilicate SiO_2 top cladding. A scheme of the channel waveguide used for successive 1D pattern is given in Fig. 1(a). The material refractive indices are slightly dispersive around the values $n_{\text{Si}_3\text{N}_4}=2$ and $n_{\text{SiO}_2}\approx n_{\text{BPSG}}=1.45$ at $1.5 \mu\text{m}$, respectively.¹⁰

1D-PhC structures are fabricated by using a 30 keV Ga⁺ focused ion beam (FIB),¹⁶ as an alternative tailor-made process well suited to the fast prototyping of high quality 1D and 2D-PhC devices.¹⁷ In our experiment, we used the LEO-ZEISS 1540XB CrossBeam®, comprising a high resolution FIB column to mill directly in combination with a high precision FEG scanning electron microscope (SEM) for precise positioning and inspection of the fabricated nanostructures in real time. The use of a patterned resist or metal masks to remove the materials is not required. Using an ion current of about 100 pA and controlling the FIB by a pattern generator (RAITH ELPHY), the pattern is directly written on the sample surface; using a total ion dose of 400 mA/cm², a depth of about $1 \mu\text{m}$ for each structure can be obtained. See Figs. 1(b) and 1(c) for FIB and SEM images of fabricated samples, respectively.

Transmission measurements are performed with an end-fire coupling scheme. The broad-band light emitted from a mercury arc lamp is first sent to a Fourier-transform spectrometer (Bruker IFS 66s) for spectral analysis. The beam is then brought to the setup via a fiber and focussed on the sample facet by means of a $25\times$ reflecting microscope objective. A second, identical objective is used to collect the light at the exit of the other waveguide facet and to refocus it onto the detector. An infrared vidicon camera allows viewing both facets of the sample for proper alignment of the waveguide on the optical axis of the measuring system. Spectra are taken in the 0.73–3 eV energy ($1.7\text{--}0.4 \mu\text{m}$ wavelength) range by means of Si and InGaAs *p-i-n* photodiodes. Light polarization is selected by means of a calcite Glan-Taylor polarizer. The spectral range on the low energy side is limited by the response of the InGaAs photodiode. Transmission through the samples is normalized to a reference channel waveguide without patterned regions.

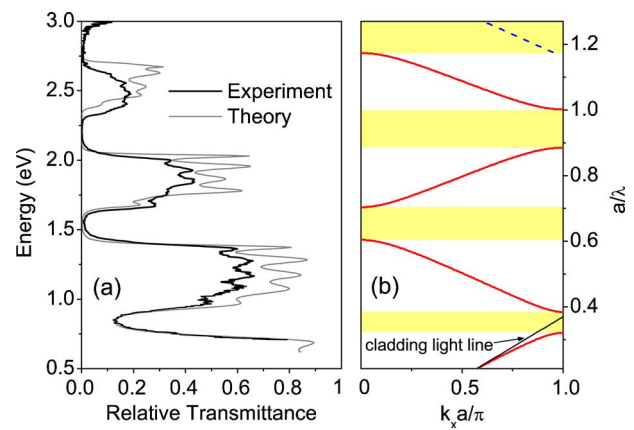


FIG. 2. (Color online) (a) Relative transmittance spectrum of TE-polarized light in the waveguide-embedded Bragg mirror shown in Fig. 1(b), compared to the calculated transmittance with parameters $L_{\text{air}}/a=0.25$, $a=525$ nm. (b) Photonic band dispersion of a 1D-PhC slab with the same parameters. Photonic band gaps of the fundamental mode are highlighted. The second-order mode of the slab waveguide (not excited in end-fire coupling experiments) is plotted with a dashed line.

The relative transmittance for the waveguide-embedded Bragg mirror is shown in Fig. 2(a).¹⁹ TE polarized light is selected at the input facet. The measured spectrum shows very well defined stop bands up to the fourth order, which increase in spectral width on increasing the energy. The relative transmission intensity in the regions outside the stop bands is pretty high, around 70% at low energy, while it rapidly decreases to below 20% for photon energies above 2.5 eV in the visible region. Fabry-Pérot oscillations (corresponding to the Bloch modes of the 1D system) are also clearly resolved in the transmitting regions. The spectra are compared to transmission calculations performed with an eigenmode expansion-based solver (FIMM-WAVE, commercial software). Eigenmode expansion¹⁸ belongs to the class of scattering matrix methods, which provide an exact solution of Maxwell equations in the frequency domain. This simulation tool is particularly suited to structures with a piecewise constant refractive index profile along the direction of light propagation, as in the present work. The simulated structure is uniform along the stripes (i.e., lateral confinement of the channel waveguide is neglected), and piecewise air slits as deep as $1.1 \mu\text{m}$ from the surface are assumed. The refractive index dispersion of the Si_3N_4 and SiO_2 materials¹⁰ is taken into account in the calculation. Notice that the effective index of the fundamental mode of the planar waveguide varies from 1.56 at 0.73 eV (close to n_{SiO_2}) up to 1.93 at 3 eV (close to $n_{\text{Si}_3\text{N}_4}$), as it results from the calculations. Very good agreement between experimental and theoretical spectra is found up to the second-order band gap. Small differences are present for energies higher than 2.2 eV, probably due to disorder effects on diffraction losses in the measured sample, and to the nonuniform width/depth ratio within the etched air slits in the BPSG cladding of fabricated samples. The decreasing of transmission intensity with increasing energies is expected from the intrinsic loss mechanism of quasiguided modes supported by the patterned slab,¹⁴ which is also evident in the calculations.

Such results are interpreted by photonic band dispersion calculations with a guided-mode expansion method,¹³ shown in Fig. 2(b).¹⁹ The simulated structure is a 1D-PhC slab with the same parameters as in the transmission calculations, but

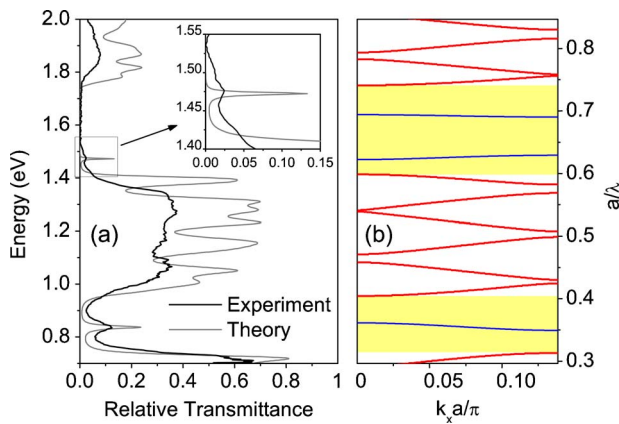


FIG. 3. (Color online) (a) Relative transmittance spectrum of TE-polarized light for the waveguide-embedded microcavity shown in Fig. 1(c), and corresponding calculated transmittance with $L_{\text{air}}/a=0.307$, $L_{\text{cav}}/a=2.91$, and $a=525$ nm. (b) Photonic band dispersion of 1D-PhC slab with a supercell in the plane. The band gap regions are highlighted.

infinitely extended in the direction of periodicity and with semi-infinite patterned claddings. Only TE modes with respect to the incidence plane are plotted. The light line of the effective cladding is also plotted (low energy range). It can be noticed that the first-order band gap lies partly below and partly above the light line. A second-order mode of the slab waveguide appears at energies above 2.7 eV (dashed line). Such mode is not excited in transmittance, owing to the symmetric spatial profile of the incoming beam. A good overall agreement can be seen with measured positions and widths of photonic gaps, even in the energy region above the light line and extending up to $a/\lambda \approx 1.25$.

By inserting a defect layer that breaks the Bragg mirror periodicity, resonant modes appear in the transmittance spectrum within the photonic stop bands, as theoretically addressed^{11,20} and experimentally shown^{3,5,7} in previous works on high index contrast systems. In Fig. 3(a), experimental results are shown for the waveguide-embedded microcavity of Fig. 1(c). Good agreement between measured and calculated TE transmittance spectra is found. A resonant cavity mode with energy 0.835 eV ($\lambda=1.485$ μm) and measured Q factor of about 22 is clearly visible within the fundamental photonic band gap. A second cavity mode is excited at energy 1.475 eV ($\lambda=0.84$ μm) within the second-order band gap (see inset of Fig. 3), with a much lower Q factor owing to the enhanced intrinsic losses and to the amplification of disorder-induced ones at shorter wavelengths. An interpretation of these spectra in terms of photonic bands is given in Fig. 3(b), where the dispersion is calculated for a structure with supercell periodicity in the slab plane. Five air slits are assumed in the supercell between two consecutive cavity layers, in order to simulate the real structure of Fig. 1(c). It is worth noting that the dispersion is represented in a reduced Brillouin zone,^{11,20} whose boundary is defined by the supercell period and it is about 0.14 in units of π/a . Cavity modes appear in the photonic band structure within the gaps. A second cavity mode is present in the second-order band gap in Fig. 3(b), but it is not evident in the measured transmittance nor in the calculated one. This is probably due to the higher intrinsic losses and lower Q factor for such a mode. It can be noticed in Fig. 3(a) that the interference pattern in the measured transmittance spectrum is less

apparent than in the calculated one. This may be attributed to an increased effect of fabrication disorder (precise air slits shape and depth) in the presence of a cavity layer that produces minigaps and low-group velocity regions in the bands of Fig. 3(b). Thus the relatively worse agreement between theory and experiment in Fig. 3(a) as compared to Fig. 2(a) stems from an increase of disorder-induced scattering for the system with the cavity.

In conclusion, 1D-PhC slabs in $\text{Si}_3\text{N}_4/\text{SiO}_2$ waveguide geometry have been successfully fabricated by FIB lithography and characterized by means of wide-band transmission spectroscopy in the near-infrared and visible ranges. The reliability of the photonic band gap concept in the quasiguided mode region and the existence of cavity modes within the band gap for structures containing defect layers have been shown. These results may be important to the realization of building elements in silicon-based photonic integrated circuits.

This work was supported by Ministero dell'Istruzione, dell'Università e della Ricerca (MIUR) through Cofin Program "Silicon-based photonic crystals," by Fondazione Banca del Monte di Lombardia, and by Provincia Autonoma di Trento (PAT) through PROFILL Project.

¹*Silicon Photonics*, Topics in Applied Physics 94, edited by L. Pavesi and D. Lockwood (Springer, Berlin, 2004).

²S. G. Johnson and J. D. Joannopoulos, *Photonic Crystals: The Road from Theory to Practice* (Kluwer, Boston, 2002).

³J. S. Foresi, P. R. Villeneuve, J. Ferrera, E. R. Thoen, G. Steinmeyer, S. Fan, J. D. Joannopoulos, L. C. Kimerling, H. I. Smith, and E. P. Ippen, *Nature (London)* **390**, 143 (1997).

⁴A. Shinya, M. Notomi, I. Yokohama, C. Takahashi, J.-I. Takahashi, and T. Tamamura, *Opt. Quantum Electron.* **34**, 113 (2002).

⁵M. Zelsmann, E. Picard, T. Charvolin, E. Hadji, B. Dal'zotto, M. E. Nier, C. Seassal, P. Rojo-Romero, and X. Letartre, *Appl. Phys. Lett.* **81**, 2340 (2002).

⁶T. F. Krauss, R. M. De La Rue, and S. Brand, *Nature (London)* **383**, 699 (1996).

⁷T. F. Krauss, B. Vögele, C. R. Stanley, and R. M. De La Rue, *IEEE Photonics Technol. Lett.* **9**, 176 (1997).

⁸D. Labilloy, H. Benisty, C. Weisbuch, T. F. Krauss, R. M. De La Rue, V. Bardinal, R. Houdré, U. Oesterle, D. Cassagne, and C. Jouanin, *Phys. Rev. Lett.* **79**, 4147 (1997).

⁹M. C. Netti, M. D. Charlton, G. J. Parker, and J. J. Baumberg, *Appl. Phys. Lett.* **76**, 991 (2000).

¹⁰J. Čtyroký, S. Helfert, R. Pregla, P. Bienstman, R. Baets, R. De Ridder, R. Stoffer, G. Klaasse, J. Petráček, P. Lalanne, J. P. Hugonin, and R. M. De La Rue, *Opt. Quantum Electron.* **34**, 455 (2002).

¹¹P. R. Villeneuve, S. Fan, S. G. Johnson, and J. D. Joannopoulos, *IEEE Proc.-J: Optoelectron.* **145**, 384 (1998).

¹²S. G. Johnson, S. Fan, P. R. Villeneuve, J. D. Joannopoulos, and L. A. Kolodziejski, *Phys. Rev. B* **60**, 5751 (1999).

¹³L. C. Andreani and M. Agio, *IEEE J. Quantum Electron.* **38**, 891 (2002).

¹⁴D. Gerace and L. C. Andreani, *Phys. Rev. E* **69**, 056603 (2004).

¹⁵N. Daldosso, M. Melchiorri, F. Riboli, M. Girardini, G. Pucker, M. Crivellari, P. Bellutti, A. Lui, and L. Pavesi, *J. Lightwave Technol.* **22**, 1734 (2004).

¹⁶K. A. Valiev, *The Physics of Sub-Micron Lithography* (Plenum, New York, 1992).

¹⁷S. Cabrini, A. Carpentiero, R. Kumar, L. Businaro, P. Candeloro, M. Prascioli, A. Gosparini, L. C. Andreani, M. De Vittorio, T. Stomeo, and E. Di Fabrizio, *Microelectron. Eng.* **78–79**, 11 (2005).

¹⁸A. S. Sudbo, *IEEE Photonics Technol. Lett.* **5**, 342 (1993).

¹⁹The energy scales of Figs. 2 and 3 are represented in both eV and a/λ units, however, notice that the photonic bands are not fully scalable with the lattice constant due to the refractive index dispersion in the wide energy range considered.

²⁰D. Gerace, M. Agio, L. C. Andreani, and Ph. Lalanne, *Opt. Quantum Electron.* **37**, 277 (2005).